Mapping global land cover in 2001 and 2010 with spatial-temporal consistency at 250 m resolution

ARTICLE *in* ISPRS JOURNAL OF PHOTOGRAMMETRY AND REMOTE SENSING · APRIL 2014

Impact Factor: 3.13 · DOI: 10.1016/j.isprsjprs.2014.03.007

6 AUTHORS, INCLUDING:

Jie Wang
Chinese Academy of Sciences
16 PUBLICATIONS **251** CITATIONS
SEE PROFILE

Yuanyuan Zhao
Tsinghua University
9 PUBLICATIONS **214** CITATIONS
SEE PROFILE

Le Yu
57 PUBLICATIONS **544** CITATIONS
SEE PROFILE

ISPRS Journal of Photogrammetry and Remote Sensing 103 (2015) 38–47

Contents lists available at ScienceDirect

ISPRS Journal of Photogrammetry and Remote Sensing

journal homepage: www.elsevier.com/locate/isprsjprs

Mapping global land cover in 2001 and 2010 with spatial-temporal consistency at 250 m resolution

Jie Wang [a], Yuanyuan Zhao [b], Congcong Li [c], Le Yu [b], Desheng Liu [d], Peng Gong [a,b,e,f,*]

[a] State Key Laboratory of Remote Sensing Science, Institute of Remote Sensing and Digital Earth, Chinese Academy of Sciences, Beijing 100101, China
[b] Ministry of Education Key Laboratory for Earth System Modeling, Center for Earth System Science, Tsinghua University, Beijing 100084, China
[c] College of Global Change and Earth System Science, Beijing Normal University, Beijing 100875, China
[d] Department of Geography, Ohio State University, Columbus, OH 43210-1361, USA
[e] Department of Environmental Science, Policy and Management, University of California, Berkeley, CA 94720-3114, USA
[f] Joint Center for Global Change Studies, Beijing 100875, China

ARTICLE INFO

Article history:
Available online 16 April 2014

Keywords:
MODIS time series data
Land cover
Change
Random forest
Markov random field
Label adjustment

ABSTRACT

Global land cover types in 2001 and 2010 were mapped at 250 m resolution with multiple year time series Moderate Resolution Imaging Spectrometer (MODIS) data. The map for each single year was produced not only from data of that particular year but also from data acquired in the preceding and subsequent years as temporal context. Slope data and geographical coordinates of pixels were also used. The classification system was derived from the finer resolution observation and monitoring of global land cover (FROM-GLC) project. Samples were based on the 2010 FROM-GLC project and samples for other years were obtained by excluding those changed from 2010. A random forest classifier was used to obtain original class labels and to estimate class probabilities for 2000–2002, and 2009–2011. The overall accuracies estimated from cross validation of samples are 74.93% for 2001 and 75.17% for 2010. The classification results were further improved through post processing. A spatial-temporal consistency model, Maximum a Posteriori Markov Random Fields (MAP-MRF), was first applied to improve land cover classification for each 3 consecutive years. The MRF outputs for 2001 and 2010 were then processed with a rule-based label adjustment method with MOD44B, slope and composited EVI series as auxiliary data. The label adjustment process relabeled the over-classified forests, water bodies and barren lands to alternative classes with maximum probabilities.

1. Introduction

Accurate global land cover data are not only critical to improving performances of ecosystem, hydrological, and climate models at the global scale (Friedl et al., 2010; Gong et al., 2013; Yang et al., 2013) but also essential to understanding the global spread of diseases from natural causes (e.g., Liang et al., 2010; Si et al., 2013). Land cover change is one of the most important factors of Earth system changes (Townshend et al., 2012). As more and more remotely sensed data become available at the global scale, global land cover products have been developed at four different resolutions including 1 km (Loveland et al., 2000; Hansen et al., 2000; Bartholomé and Belward, 2005; Tateishi et al., 2011), 500 m (Friedl et al., 2002; 2010), 300 m (Arino et al., 2008; Bontemps et al., 2010), and 30 m (Gong et al., 2013; Yu et al., 2013a). Most of the land cover products were produced for a single year with different classification algorithms or classification systems. The MODIS 500 m land cover products were generated on an annual basis by using a supervised boosted decision tree classifier. The 300 m GLOBcover land cover data were produced for 2005 and 2009, respectively, using spectral-temporal and phenological information with an unsupervised classification method. The 30 m finer resolution observation and monitoring of global land cover (FROM-GLC) data were produced with supervised classification using Landsat Thematic Mapper (TM) and enhanced TM plus (ETM+) data as input with various machine learning algorithms (Gong et al., 2013). However, FROM-GLC data were only based on a single date Landsat image for a particular pixel. Therefore the land cover information produced with the 30 m product may not reflect the dominant land cover type of a particular year. To overcome this problem, coarser resolution time-series have been combined with the 30 m data through an approach consisting of image segmentation and random forest classification (Yu et al., 2013a).

* Corresponding author at: Center for Earth System Science, Tsinghua University, Beijing 100084, China.
E-mail address: penggong@tsinghua.edu.cn (P. Gong).

http://dx.doi.org/10.1016/j.isprsjprs.2014.03.007
0924-2716/

Among all the global land cover products, image classification was done based on spectral-temporal information available to a particular classification unit. Potential information in the spatial–temporal context, which is useful for consistency checking and noise removal, has not been applied.

At the local and regional scale, multi-year data were used to derive land cover information with an assumption of no land cover change (Hüttich et al., 2011). If land cover of a single year is the concern, information from the preceding and subsequent year can also be used to improve classification accuracy. Markov Random Field (MRF) models were used in Liu et al. (2006, 2008) to model the spatial–temporal dynamics of two co-registered images, and were used in Liu and Cai (2012) to reconstruct land cover change trajectories in multiple years from multi-temporal Landsat data. Mapping results were optimized by using spatial–temporal neighborhood information with the MRF model. As a by-product, classifiers such as support vector machines (SVM) or random forests can output estimations of class probability (Wu et al., 2004; Breiman, 2001). The estimated class probabilities were used as likelihood estimation of a pixel in the MRF model. However, at the global scale, none of these approaches have been tested due to the lack of suitable training and test samples.

Auxiliary data and prior knowledge are important in improving classification accuracies. The elevation data and geographical coordinates are often used as auxiliary inputs (e.g. Homer et al., 2007). Such information has also been used directly or indirectly in some rule based or hierarchical classification processes to obtain better mapping results (Thenkabail et al., 2009; Sulla-Menashe et al., 2011; Yu et al., 2013b). Again, these methods have not been tested at the global scale.

In this research, we evaluated the spatial-temporal contextual approach in global land cover mapping with 250 m resolution MODIS time series data. Samples were selected from the FROM-GLC project (Gong et al., 2013; Zhao et al., submitted for publication). MODIS vegetation index data as well as four spectral bands of MODIS collection 5, MOD13Q1, were used as the main inputs. Information from the preceding and subsequent years was used to improve classification accuracy of the current year with the MRF model. A rule-based label adjustment process was performed with the multi-year land cover data, estimated class probability and auxiliary data as inputs. Impervious surfaces were not mapped in this research as they are of small areas at the global scale and are often mixed with other types at resolutions of MODIS data. Specialized methods as applied in other studies (Gong and Howarth, 1990; 1992; Schneider et al., 2009; 2010) are being investigated for mapping fractional cover of impervious surfaces.

2. Material and methods

2.1. Classification system

The classification system used here was derived from Gong et al. (2013), and modified with respect to properties of MODIS data. A two-level land cover classification system was designed in Gong et al. (2013), including 29 Level 2 classes, which could be merged into 11 Level 1 classes. The designed system can be easily cross-walked to the land cover classification systems of the United Nations Food and Agriculture Organization (FAO) Land Cover Classification System (LCCS) and the classification system of the International Geosphere–Biosphere Programme (IGBP). Cross-walking for some classes need additional layers of information, such as fractional cover, vegetation height, and phenological properties of vegetation that can be derived from time-series data.

We determined land cover categories considering MODIS time series for a whole year, so transient classes were modified accordingly. For example, the original "Bare Croplands" was changed to "Seasonal croplands", and merged into Level 1 class "Croplands". The "Other barren lands" and "Cloud" classes were removed. The Level 1 "Wetlands" class was not included here because of spectral variability due to temporal variation of water levels. The "Impervious" class is difficult to classify directly at 250 m resolution, and it was dropped from the classification system. We are investigating alternative mapping methods for these special categories. The revised classification system is composed of 25 Level 2 classes merging into 7 Level 1 classes, as shown in Table 1.

2.2. Data

To map global land cover in 2001 and 2010, MOD13Q1 time series for 2000, 2001, 2002, 2009, 2010 and 2011, slope data and latitude were used. The MODIS Vegetation Continuous Fields (VCF) product (MOD44B; DiMiceli et al., 2011), for 2001 and 2010 was used in post classification processing.

MOD13Q1 data in MODIS Collection 5 are provided every 16 days at nominal 250 m resolution. The MOD13Q1 data contains an Enhanced Vegetation Index (EVI), a Normalized Difference Vegetation Index (NDVI), 4 spectral bands (RED (620–670 nm), NIR (841–876 nm), BLUE (459–479 nm), and MIR (2105–2155 nm)), a quality control layer and other information layers. The BLUE and MIR bands are resampled from 500 m resolution to 250 m. There are 296 tiles of MOD13Q1 covering global land areas (excluding Antarctica). EVI includes information in the blue band to make it less sensitive to soil and atmospheric effects than NDVI (Waring et al., 2006). Thus, we selected EVI and the 4 spectral bands as the main input data.

The slope data were computed from digital elevation model (DEM) data in the Shuttle Radar Topographic Mission (SRTM) dataset (Jarvis et al., 2008) and the GTOPO30 dataset (http://eros.usgs.gov/#/Find_Data/Products_and_Data_Available/gtopo30_info). The SRTM DEM has a resolution of 90 m at the equator and covers up to 60 degrees north and south. The GTOPO30 DEM is of 30-arc seconds (approximately 1 km at the Equator) resolution, and was used as a supplement where the SRTM DEM does not have coverage.

MOD44B (the VCF product) is derived yearly at 250 m resolution. It contains a percent tree cover layer, a quality layer, a percent tree cover standard deviation (SD) layer and a cloud layer. Values in the percent tree cover layer are estimated percentage of pixel

Table 1
Classification system.

Level1	Class names	Level 2				
		1	2	3	4	5
1	Croplands	Rice fields	Greenhouse farming	Other croplands	Seasonal croplands	Pastures
2	Forests	Broadleaf forests	Needleleaf forests	Mixed forests	Orchards	
3	Grasslands	Marshland	Herbaceous tundra	Other grasslands		
4	Shrublands	Shrub and brush tundra	Other shrublands			
5	Water bodies	Lake	Reservoir/pond	River	Ocean	
6	Barren lands	Dry salt flats	Sandy areas	Exposed bare rock	Dry lake/river bottoms	Tidal area
7	Snow/ice	Snow	Ice			

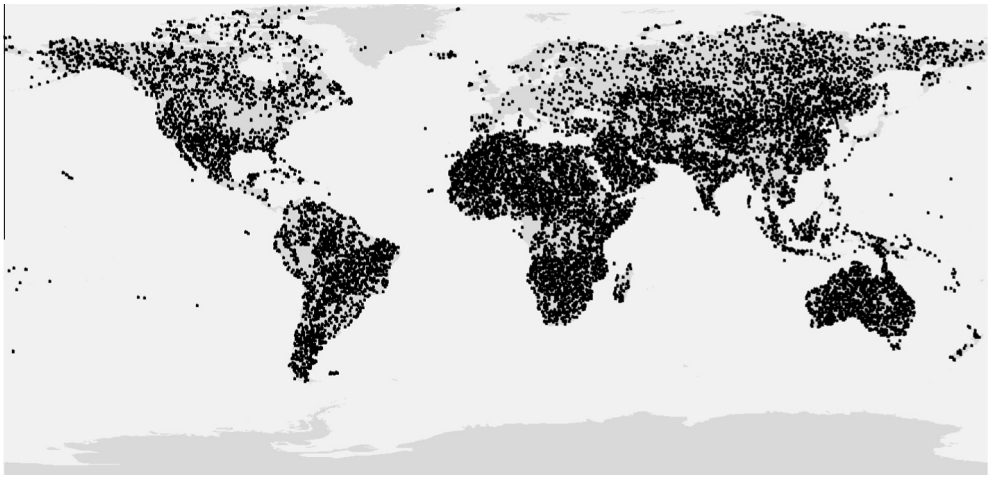

Fig. 1. Spatial distribution of samples.

area covered by tree (integers from 0 to 100 for valid range, 200 for water and 253 for fill value). The VCF data correspond pixel-by-pixel to the MOD13Q1 data, and we used them to filter out misclassified forests. Validation has been performed for the last version of MOD44B using data from field sites in Maryland, United States and Mato Grosso, South America (http://glcf.umd.edu/library/guide/VCF_C5_UserGuide_Dec2011.pdf). The root mean square errors (RMSEs) were 9.74% and 10.46%, and the mean absolute errors were 7.87% and 9.40% over the two sites, respectively.

2.3. Training samples

Our training samples are selected from the FROM-GLC project (Gong et al., 2013; Zhao et al., submitted for publication). The training samples were interpreted and cross-checked based on Landsat TM and Google Earth data, and then rechecked twice by high quality image interpreters using EVI time series for 2010 as auxiliary data. The validation samples were preset in a systematic unaligned manner, and then were interpreted and checked by high quality image interpreters. As a final step, one of the best interpreters finalized the validation samples to further improve accuracy and consistency.

The original samples are based on Landsat TM at 30 m resolution. The *large samples* in Gong et al. (2013) and Zhao et al. (submitted for publication) are those with homogeneous areas greater than 500 m × 500 m. We used only the large samples in the 250 m MODIS classification. For classes with few large validation samples, large training samples were also used. The spatial distribution of the samples is shown in Fig. 1. Fig. 2 shows the number of samples for each class. The sample numbers of different classes differ significantly. Despite this undesirable proportional distribution it is the best sample currently available.

2.4. Data and sample preparation

Fig. 3 shows a flowchart of the methodology for data and sample preparation. More detail is presented in the following subsections.

2.4.1. Data preparation

We first set the cloudy pixels of EVI, RED, NIR, BLUE and MIR time series from MOD13Q1 to missing values, and smoothed the data with a method based on the Savitzky–Golay filter (Chen et al., 2004). Then, time series in each band were aggregated to 32-day averages. The averaging reduces data volume and helps to improve classification accuracy (Friedl et al., 2010; Hüttich et al., 2011).

The DEM data were reprojected, sampled and gridded to the MODIS tiles, so that the resultant data were registered pixel-to-pixel to the tiles of MOD13Q1. Abnormally high values appear at the land–ocean boundary when computing the slope data from the DEM data, these values were replaced with zeroes. For each MOD13Q1 tile, we computed latitude for all pixels and saved them in an input layer. In total, there are 62 input features for a single year, including monthly EVI (12), monthly spectral bands (12∗4), slope (1) and latitude (1).

2.4.2. Sample change in time

The original samples were collected for the year 2010. Based on the geographical location, we compared samples in other years

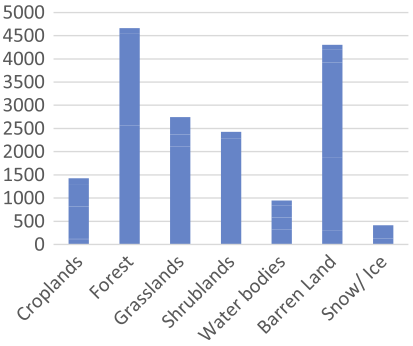

Fig. 2. Sample distribution by class.

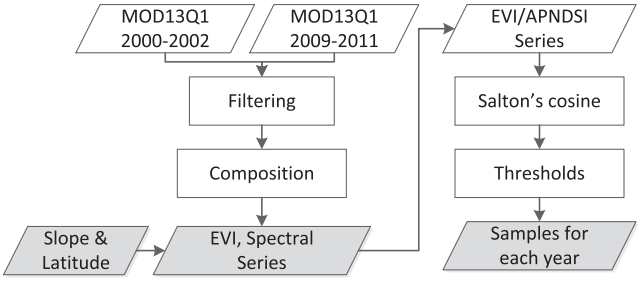

Fig. 3. Data preparation and sample selection.

Table 2
Number of samples for each year.

	Croplands	Forest	Grasslands	Shrublands	Water bodies	Barren lands	Snow/ice	Total num
2000	1318	4112	2416	2135	838	4085	367	15,271
2001	1313	4112	2416	2135	838	4109	368	15,291
2002	1308	4115	2416	2135	838	4085	368	15,265
2009	1327	4118	2416	2135	838	4072	367	15,273
2010	1358	4164	2609	2305	904	4150	396	15,886
2011	1315	4116	2416	2135	838	4082	367	15,269

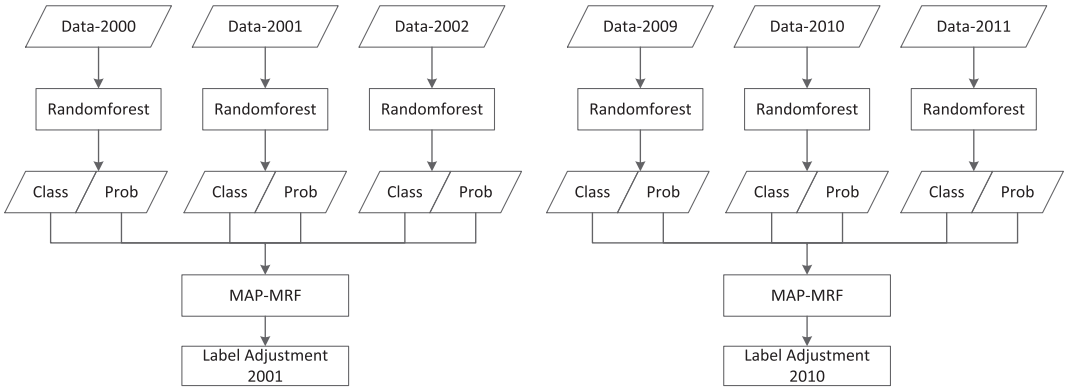

Fig. 4. Land cover mapping workflow.

with samples for 2010 to detect changes. The monthly EVI data were used as the main input vectors for change detection. The EVI values are also high in snow-covered regions (Huete et al., 2002), so it is difficult to detect snow/vegetation transitions. For snow/ice samples, we used the approximate normalized difference snow and ice index (APNDSI) instead of the EVI. The APNDSI is an approximation of NDSI (Xiao et al., 2001) defined as

$$APNDSI = \frac{\mathrm{RED} - \mathrm{MIR}}{\mathrm{RED} + \mathrm{MIR}}$$

where RED and MIR are spectral bands from MOD13Q1. Salton's cosine, which is in close relation with the correlation coefficient (Egghe and Leydesdorff, 2009), was used to measure vector similarity. Salton's cosine of two vectors A, B is defined as

$$\cos(A,B) = \frac{\sum_{i=1}^{n} A_i B_i}{\sqrt{\sum_{i=1}^{n} A_i^2}\sqrt{\sum_{i=1}^{n} B_i^2}}$$

where n is the length of the vector (12 in our case), and A_i is the *ith* element of A. We manually set the thresholds to determine change/no-change for each class of each year. Samples for year 2010 were also filtered to remove a few unstable points. The unchanged samples were used to train the classifier for the corresponding year. Table 2 shows the number of samples (for Level 1 classes) for each year.

2.5. Land cover mapping method

We mapped the global land cover data into Level 2 classes, and the results were merged into Level 1 classes when needed. With data from adjacent years, we used a spatial-temporal consistency model, Maximum a Posteriori Markov Random Fields (MAP-MRF) (Liu et al., 2006, 2008; Liu and Cai, 2012), to improve the land cover classification. Finally, we performed a fine label adjustment on the output data for 2001 and 2010. Fig. 4 shows the land cover mapping workflow.

For each of the six years, a random forest (Breiman 2001) classifier of 200 trees was trained, with the slope, the latitude, the monthly EVI and the monthly spectral bands as input features.

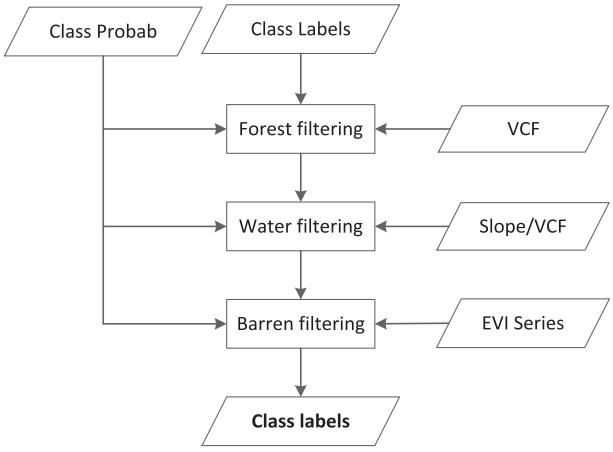

Fig. 5. Rule-based label adjustment.

The trained classifier was then applied to all the pixels to get the class labels and the posterior probabilities. The posterior probability estimated by the random forest classifier indicates a pixel's probability of belonging to a class given the input features. A pixel's class label is determined according to the maximum probability value.

The MAP-MRF model was applied to the probabilities of the 3 consecutive years to improve the accuracy and consistency of the land cover classification. The model is defined and computed in the same way as in Liu and Cai (2012). Using the *Iterated conditional modes* (ICM) algorithm (Besag, 1986), the solution can be obtained by iteratively maximizing the conditional posterior probability of each pixel. For a pixel of spatial-temporal position (s, t), the resultant label is computed:

$$L^*_{(s,t)} = \arg\max_{L_{(s,t)}} \{P(L_{(s,t)} | L_{\mathbb{N}}(s,t)) * f(X_{(s,t)}) | L_{(s,t)}\}$$

where X is the data; L is the class label; $\mathbb{N}(s,t)$ is the set of spatial-temporal neighbors for pixel (s, t); f is the marginal likelihood

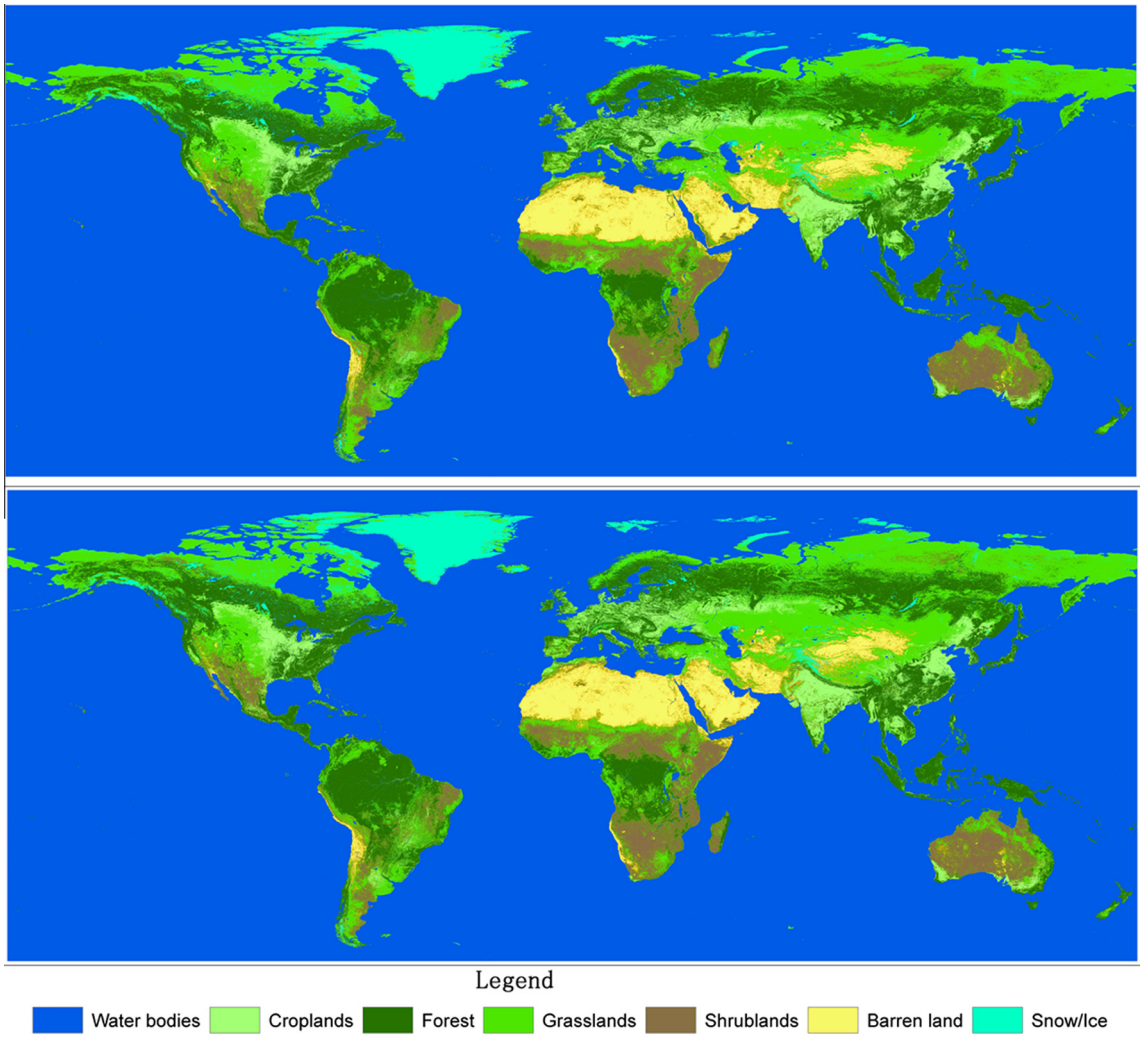

Fig. 6. Global mapping results for 2001 (top) and 2010 (bottom).

function at pixel (s, t), estimated by the classifier as probabilities for all given labels; and P is the conditional prior distribution computed from the spatial-temporal relationship:

$$P(L_{(s,t)}|L_{\mathbb{N}(s,t)}) = \frac{1}{Z}\exp\{-[U_s + U_{T1} + U_{T2}]\}$$

where Z is a normalizing constant, U_S is called the spatial energy function, $U_{T1}$is called the temporal energy function for the past and U_{T2} for the future. Maximum a posteriori probability is often converted to energy minimization in solving the MRF models. The energy functions are defined as:

$$U_s = \sum_{(s',t')\epsilon\mathbb{N}_{s(s,t)}} [-\beta_1 I(L_{(s,t)} = L_{(s',t')})],$$

$$U_{T1} = \sum_{(s',t')\epsilon\mathbb{N}_{T1(s,t)}} [-\beta_2 P(L_{(s,t)}|L_{(s',t')}) + \beta_3 I(L_{(s',t')} \nRightarrow L_{(s,t)})],$$

$$U_{T2} = \sum_{(s',t')\epsilon\mathbb{N}_{T2(s,t)}} [-\beta_4 P(L_{(s',t')}|L_{(s,t)}) + \beta_5 I(L_{(s,t)} \nRightarrow L_{(s',t')})],$$

where β is the nonnegative coefficient; $I(X)$ is an indicator function that is equal to 1 if X is true and 0 otherwise; $L_1 \nRightarrow L_2$ means an illogical transition; and $P(L_2|L_1)$ is the temporal transition probability from L_1 to L_2. We computed the model tile by tile. The temporal transition probability matrices were estimated based on the global transition model (Liu et al., 2008), and by counting pixel pairs within each tile.

2.6. Rule based label adjustment

Although input samples are critical to final classification accuracy, it is impossible to include all variations with training samples at the global scale. The MAP-MRF process can improve the accuracy and consistency of land cover maps, but there is still a need for label adjustment based on prior knowledge and/or auxiliary data. The process of post classification label adjustment is shown in Fig. 5.

For each pixel, the corresponding probabilities estimated by the random forest classifier were used to find the most probable new label when the pixel's label was to be changed. The alternative class with the maximum probability value was selected as the new label.

We first filtered the output data with the percent tree cover of the VCF data. A pixel of the VCF data was regarded as forest if the percent tree cover value was in $[t, 100]$, where t is the given threshold. The forest/nonforest threshold was derived from comparing the VCF data for 2010 and the FAO global forest cover statistics 2010 (FRA, 2010). The forest area of the VCF data is closest to the FRA 2010 results, 4 billion ha, when the threshold value is set to 21. We selected the value 18, so that the forest area of the filtered

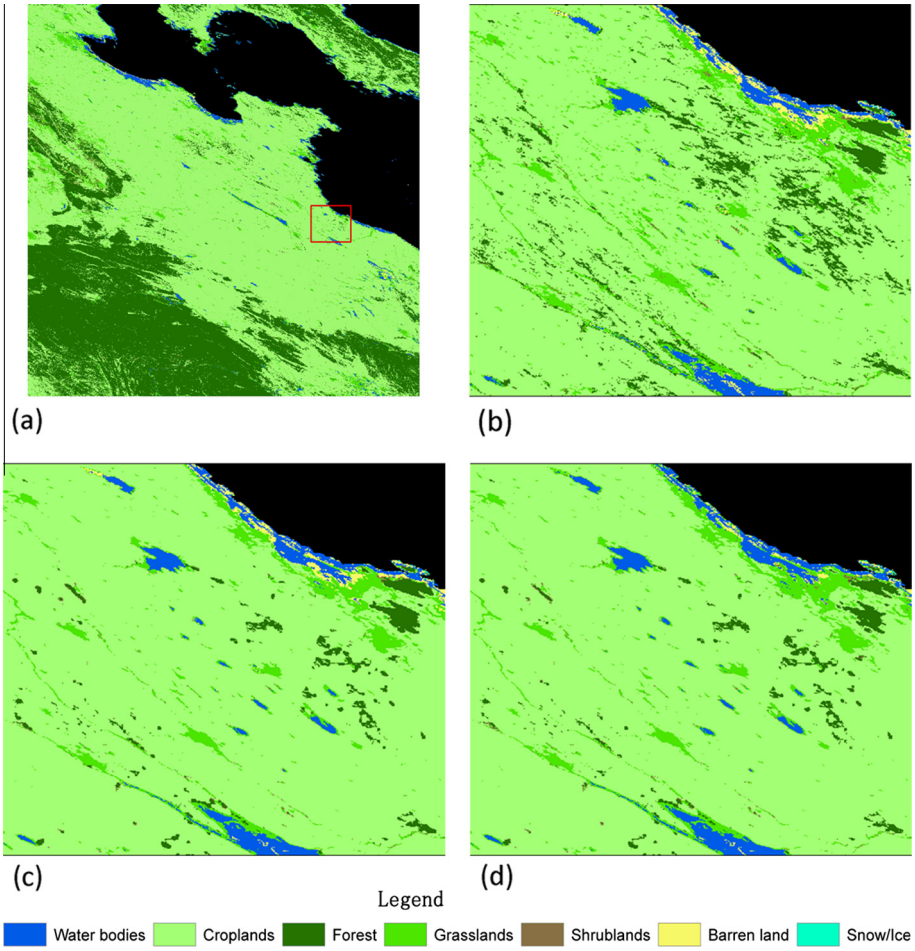

Fig. 7. Regional results for the year 2010 in North China Plain. (a) Land cover in MODIS tile h27v05, the red box indicates the area shown in b–d, (b) output from random forest, (c) Output from MAP-MRF, and (d) output from label adjustment. (For interpretation of the references to colour in this figure legend, the reader is referred to the web version of this article.)

land cover mapping in 2010 was close to the FRA 2010. For 2001 and 2010, if a pixel was classified as forest and the percent tree cover value was less than 18 or greater than 100, then its label would be changed to the second most likely class after forests.

Pixels with a large proportion of shadows located in mountain areas were often classified as water bodies. We filtered all water bodies with the slope data. If a pixel was labeled as water body and the corresponding slope was greater than a given threshold, it would be relabeled to the second most likely class after water bodies. If the corresponding VCF value was not between 18 and 100, forest would not be chosen as a substitute to water bodies. The threshold of slope was set manually tile-by-tile with visual interpretation. All threshold values are around 10 degrees, and the fine-tuning was performed to reduce errors between misclassified water bodies and real water bodies.

Finally, we filtered *barren lands* (Level 2 classes) with EVI data. If the average of the two highest EVI values was greater than a given threshold, we would compare the probability values of grasslands (Level 2 classes) and shrublands (Level 2 classes). If the maximum probability value was also greater than a given threshold, the label would be changed to the corresponding class. The thresholds were set manually tile-by-tile with visual interpretation.

3. Results and discussions

Fig. 6 shows the global mapping results for 2001 and 2010. Tremendous changes in regional area are often inconspicuous at the global scale. Deforestations in the Amazon River Basin and West Africa, forest restoration in South China are cases of dramatic land cover changes. In Africa, croplands are under-classified, and are confused with grasslands and shrublands for both years. One cause is the lack of large cropland samples in that region. The cropland fields are often cultivated in small patches, and are sparsely scattered within large areas of forest or grassland in Sub-Sahara Africa (You et al., 2009).

The MAP-MRF algorithm is a process for optimizing land cover classification with information from spatial-temporal neighborhoods. Although the spatial consistency is less significant at 250 m resolution than those at finer resolutions, the temporal neighbors can still provide important information. Thus the classification accuracy can be improved with the MAP-MRF algorithm. Fig. 7 shows regional results for the year 2010. The region is located in the North China Plain, as indicated in Fig. 7a (MODIS tile h27v05) with a red box. Croplands are the main land cover type in this region. Some over-classified forests were correctly relabeled as croplands by using the MAP-MRF model and the label adjustment further refined some details.

Label adjustment based on prior knowledge and auxiliary data can be used to eliminate confusion caused by poorly distributed samples or imbalanced sample numbers, and to reduce the impact of large mountain shadows. This can be partly seen from Fig. 7d where a few pixels were relabeled from forests or barren lands to other classes. Fig. 8 shows regional results for the year 2010 in Tibet. The region of interest is indicated with a red box in Fig. 8a (MODIS tile h25v06). Pixels with a large proportion of shadows,

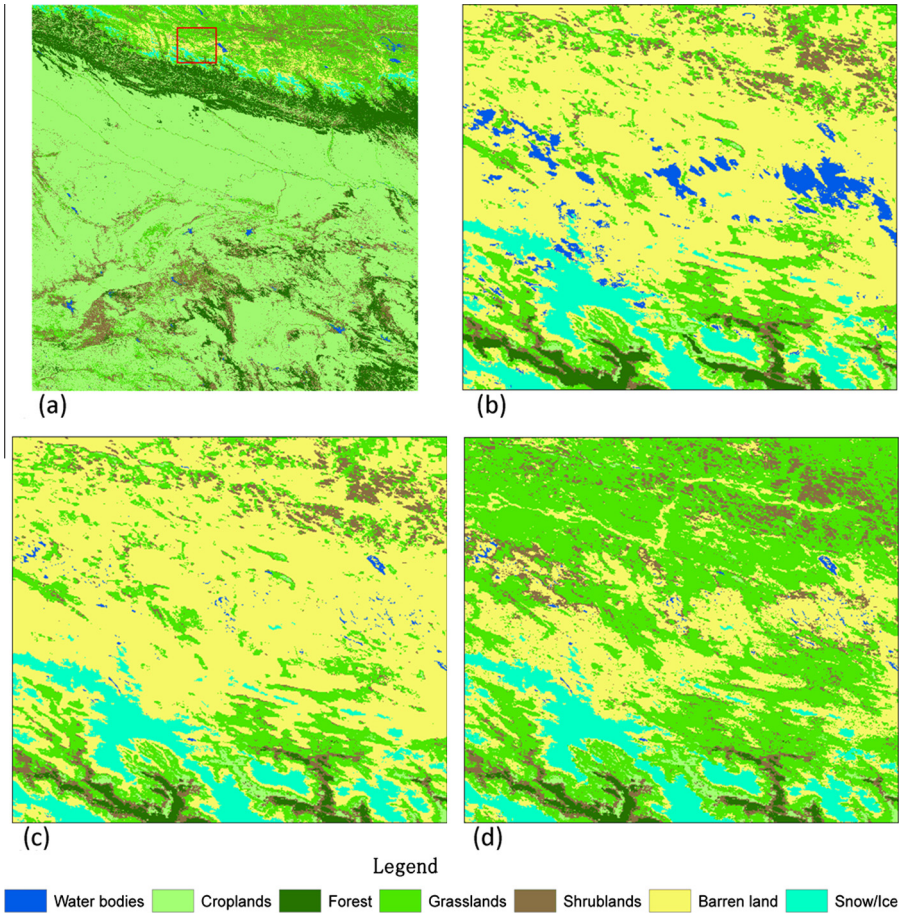

Fig. 8. Regional results for the year 2010 in Tibet. (a) and cover of a MODIS tile with identifier h25v06, red box indicates the range of the sample region, (b) output from MAP-MRF, (c) output from water filtering, and (d) output from barren filtering.

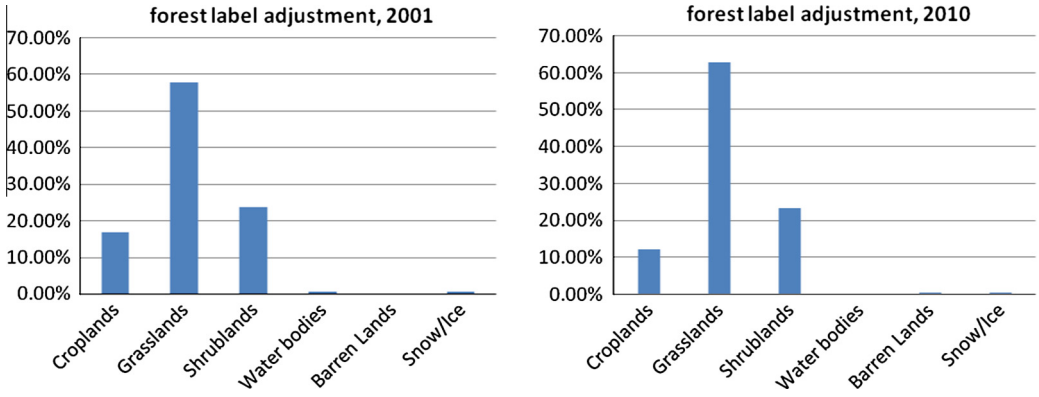

Fig. 9. Classes relabeled from forests after forest filtering for 2001 (left) and 2010 (right).

especially those located in large mountain areas, were often classified as water bodies. These were not corrected by the MAP-MRF model, as shown in Fig. 8b. After water filtering, most incorrectly classified water bodies were eliminated. However, a small fraction of incorrectly classified water pixels still exists. These pixels contain large proportions of shadows, but their corresponding slope values are low. The final results Fig. 8d were obtained from barren lands filtering. Grasslands and shrublands with weak vegetation signals were separated from the barren lands.

Globally, over-classified forests were changed to grasslands, shrublands, croplands and other classes by label adjustment. By forest filtering, about 8,926,510 km^2 of forests for 2010 and 10,129,466 km^2 for 2001 were relabeled to other classes. Fig. 9 shows the percentage of each class in relabeled pixels from forests after forest filtering. Grasslands, shrublands and croplands are easily confused with forests, and the bar plots for 2001 and 2010 are similar in shape.

About 84,980 km^2 of water bodies for 2010, and 120,230 km^2 for 2001 were identified as other cover types with a large proportion of shadows. Fig. 10 shows the percentage of each class relabeled from water. The blue bars represent the percentage of cover types in the relabeled water pixels, and the red bars

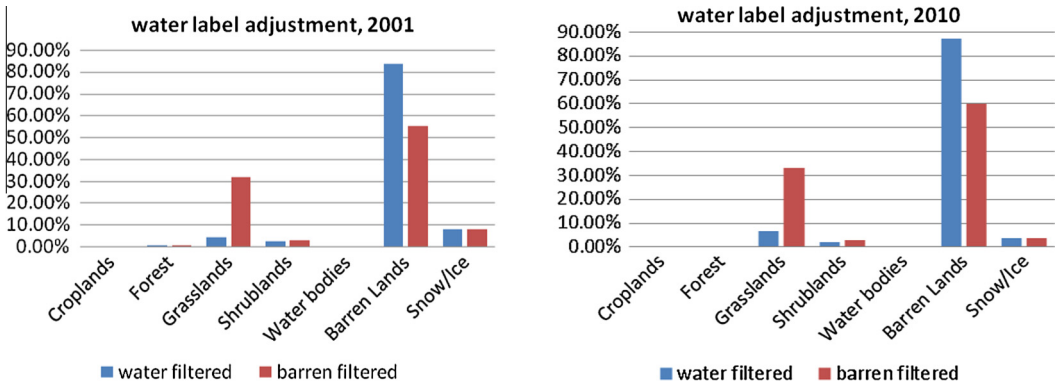

Fig. 10. Classes relabeled from water in water filtering for 2001 (left) and 2010 (right). The blue bars are percentage of cover types relabeled after water filtering, and the red bars are the results after some barren lands are relabeled.

Table 3
Stratified 10-fold cross validation estimation for 2001 (Overall Accuracy: 74.93%, Kappa: 0.6850. CR = Croplands, FR = Forests, GR = Grasslands, SHR = Shrublands, WB = Water bodies, BR = Barren lands, SI = Snow/Ice).

Name	CR	FR	GR	SHR	WB	BR	SI	Total Num	UA (%)
CR	**633**	78	70	29	2	16	0	828	76.45
FR	151	**3595**	346	300	5	10	7	4414	81.45
GR	279	170	**1330**	342	24	184	68	2397	55.49
SHR	188	267	475	**1297**	8	214	0	2449	52.96
WB	4	0	11	1	**703**	43	9	771	91.18
BR	58	2	172	160	55	**3622**	6	4075	88.88
SI	0	0	12	6	41	20	**278**	357	77.87
Total num	1313	4112	2416	2135	838	4109	368	**15,291**	
PA (%)	48.21	87.43	55.05	60.75	83.89	88.15	75.54		**74.93**

Significance of bold values is used to highlight the sample numbers correctly predicted, and to highlight total sample number and overall accuracy.

Table 4
Stratified 10-fold cross validation estimation for 2010 (Overall Accuracy: 75.17%, Kappa: 0.6897. CR = Croplands, FR = Forests, GR = Grasslands, SHR = Shrublands, WB = Water bodies, BR = Barren lands, SI = Snow/Ice).

Name	CR	FR	GR	SHR	WB	BR	SI	Total num	UA (%)
CR	**670**	65	66	22	2	15	3	843	79.48
FR	128	**3607**	347	308	2	10	11	4413	81.74
GR	316	191	**1497**	372	9	166	67	2618	57.18
SHR	183	299	521	**1425**	0	237	0	2665	53.47
WB	5	0	11	1	**792**	39	11	859	92.20
BR	56	1	153	175	51	**3659**	12	4107	89.09
SI	0	1	14	2	48	24	**292**	381	76.64
Total num	1358	4164	2609	2305	904	4150	396	**15,886**	
PA (%)	49.34	86.62	57.38	61.82	87.61	88.17	73.74		**75.17**

Significance of bold values is used to highlight the sample numbers correctly predicted, and to highlight total sample number and overall accuracy.

represent the percentage of cover types in the relabeled barren lands pixels. The pixels with a large proportion of shadows located in large mountain areas are mostly barren lands. There are also some grasslands and shrublands with weak vegetation signals, and some snow/ice in the high altitude area.

Training samples are always expensive to obtain for global land cover mapping and an independent validation sample set requires a tremendous amount of time to acquire. Friedl et al. (2010) measured the map accuracy by performing a 10-fold cross validation with an effort to avoid spatial autocorrelation. Their samples were from thousands of polygons. Our samples were independent points. With the random forest classifier, we estimated the map accuracy with a stratified 10-fold cross validation directly. Table 3 is the confusion matrix for 2001 and Table 4 for 2010. Croplands, grasslands and shrublands tend to be confused with each other, and barren lands and water bodies have high accuracies. Forests and shrublands classes are somewhat over-classified, and the croplands class is under-classified in the results derived directly from supervised classification. We also performed stratified cross validation for 2000, 2002, 2009, and 2011. The overall accuracy values are 74.95%, 75.13%, 75.25%, and 74.62%, respectively. The out-of-bag (OOB) error can be estimated as an accuracy measurement when training the random forest with all samples (Breiman, 2001). The OOB error estimated for Level 2 classes is 0.3769 for 2001, and 0.3781 for 2010.

The overall accuracy for 2010 estimated for Level 2 classes is 62.48%. Mixed forests tend to be confused with other Level 2 classes of forests. Seasonal croplands exhibits low producer's accuracy, and they were mainly misclassified to other croplands. Dry lake/river bottoms were mainly misclassified to dry salt flats and exposed bare rock.

With 2010 data we also assessed the contribution of each step of post-processing to the improvement of image classification. We used 80% of the total samples for training and the remaining 20% for testing. The overall accuracy was 74.30% for outputs directly from random forest and 82.07% for outputs from MAP-MRF. The inclusion of spatial–temporal contextual information has clearly increased the overall classification accuracy. However,

during the label adjustment process, the overall accuracies decreased. They were 80.09%, 80.06% and 75.31% for outputs of forest filtering, water filtering and barren filtering. When the label adjustment was performed directly to the outputs of random forest, the overall accuracy for the final results was only 70.53%. This indicates MAP-MRF is helpful for improving land cover classification with auxiliary data from the preceding and subsequent years. The main reason for accuracy decrease during the label adjustment process is because the properties of some land cover classes in the training samples have been changed to other classes through label adjustment. The training samples used in this study were originally collected for classification with Landsat TM data. Some samples were collected from Landsat images acquired outside of the growing season. Thus such samples have been identified as barren lands. The label adjustment would convert them to vegetative categories. In addition, the forest class includes any land in the image when greater than 10% tree cover is estimated by an image analyst but when we apply the label adjustment, a higher percentage (18%) of tree cover from VCF has been used in accordance with FAO statistics. The MRF processes are consistent with information from training samples, but the label adjustment can correct for sample inconsistency and bias in the classification.

4. Summary

Using MOD13Q1 data for 2000, 2001, 2002, 2009, 2010 and 2011, slope data and latitude coordinates as inputs, we mapped the global land cover for 2001 and 2010 at 250 m resolution. Samples for each year were those unchanged between 2000 and 2010 as determined with a change detection algorithm. A MAP-MRF model was used to get consistent results with the auxiliary data from the preceding and subsequent years of 2001 and 2010. A rule-based label adjustment was performed to reduce the impact of poorly distributed samples and topography. This algorithm can be applied to any particular year when MODIS time series data of three consecutive years are available.

Considering the diversity of global land cover, regional information and knowledge will be helpful in improving classification accuracies. The number of samples and the distribution of samples in the feature space are important for good mapping results. We need more training and validation points to further improve the classification accuracies of the global land cover maps. It is desirable to reinterpret samples in years other than 2010, especially for those changed samples. Since the croplands in Africa tend to be confused with other vegetation cover types, more cropland samples and auxiliary data should be collected in this region.

To make better use of MAP-MRF model, it is critical to accurately estimate the transition probability. The transition probability estimation with the wall-to-wall statistics of the temporal neighbors is a compromise of accuracy and computing efficiency (Liu et al., 2008), and should be replaced by a more effective method.

Inland water bodies are highly dynamic even in a single year and may only exist for a short period annually. New concepts such as the dynamic land cover type proposed in a recent research (Sun et al., in press) may prove effective for mapping such ephemeral land cover classes.

Acknowledgements

We are grateful to Dr. Nicholas Clinton for his comments and editing of an earlier draft of this paper. This research was partially supported by a National High Technology Research and Development Program of China (2013AA122804), a National Natural Science Foundation of China (41001274), a research grant from Tsinghua University (2012Z02287) and the "135" Strategy Planning grant of the Institute of Remote Sensing and Digital Earth, CAS (Y3SG1500CX).

References

Arino, O., Bicheron, P., Achard, F., Latham, J., Witt, R., Weber, J.L., 2008. GLOBCOVER The most detailed portrait of Earth. ESA Bulletin–European Space Agency 136, 24–31.

Bartholomé, E., Belward, A.S., 2005. GLC2000: a new approach to global land cover mapping from Earth observation data. Int. J. Remote Sensing 26, 1959–1977.

Besag, J., 1986. On the statistical analysis of dirty pictures. J. R. Statist. Soc. Ser. B (Methodological), 259–302.

Bontemps, S., Defourney, P., Van Bogaert, E., Arino, O., 2010. GLOBCOVER2009 products description and validation report. <http://globcover.s3.amazonaws.com/LandCover2009/GLOBCOVER2009_Validation_Report_1.0.pdf>.

Breiman, L., 2001. Random forests. Mach. Learn. 45, 5–32.

Chen, J., Jönsson, P., Tamura, M., Gu, Z., Matsushita, B., Eklundh, L., 2004. A simple method for reconstructing a high-quality NDVI time-series data set based on the Savitzky–Golay filter. Remote Sensing Environ. 91 (3), 332–344.

DiMiceli, C.M., Carroll, M.L., Sohlberg, R.A., Huang, C., Hansen, M.C., Townshend, J.R.G., 2011. Annual Global Automated MODIS Vegetation Continuous Fields (MOD44B) at 250 m Spatial Resolution for Data Years Beginning Day 65, 2000–2010, Collection 5 Percent Tree Cover. University of Maryland, College Park, MD, USA.

Egghe, L., Leydesdorff, L., 2009. The relation between Pearson's correlation coefficient r and Salton's cosine measure. J. Am. Soc. Inform. Sci. Technol. 60, 1027–1036.

FRA 2010. Global Forest Resources Assessment 2010 (Food and agriculture organization of the United Nations, 2010). <http://www.fao.org/forestry/fra/fra2010/en/>.

Friedl, M.A., Mciver, D.K., Hodges, J.C.F., Zhang, X.Y., Muchoney, D., Strahler, A.H., Woodcock, C.E., Gopal, S., Schneider, A., Cooper, A., Baccini, A., Gao, F., Schaaf, C., 2002. Global land cover mapping from MODIS: algorithms and early results. Remote Sensing Environ. 83, 287–302.

Friedl, M.A., Sulla-Menashe, D., Tan, B., Schneider, A., Ramankutty, N., Sibley, A., Huang, X., 2010. MODIS Collection 5 global land cover: algorithm refinements and characterization of new datasets. Remote Sensing Environ. 114, 168–182.

Gong, P., Howarth, P.J., 1990. The use of structural information for improving land-cover classification accuracies at the rural-urban fringe. Photogrametric Eng. Remote Sensing 56 (1), 67–73.

Gong, P., Howarth, P.J., 1992. Frequency-based contextual classification and grey-level vector reduction for land-use identification. Photogrametric Eng. Remote Sensing 58 (4), 423–437.

Gong, P., Wang, J., Yu, L., Zhao, Y., Zhao, Y., Liang, L., Niu, Z., Huang, X., Fu, H., Liu, S., Li, C., Li, X., Fu, W., Liu, C., Xu, Y., Wang, X., Cheng, Q., Hu, L., Yao, W., Zhang, H., Zhu, P., Zhao, Z., Zhang, H., Zheng, Y., Ji, L., Zhang, Y., Chen, H., Yan, A., Guo, J., Yu, L., Wang, L., Liu, X., Shi, T., Zhu, M., Chen, Y., Yang, G., Tang, P., Xu, B., Ciri, C., Clinton, N., Zhu, Z., Chen, J., Chen, J., 2013. Finer Resolution Observation and Monitoring of Global Land Cover: First Mapping Results with Landsat TM and ETM+ Data. Int. J. Remote Sensing 34, 2607–2654.

Hansen, M.C., Defries, R.S., Townshend, J.R.G., Sohlberg, R., 2000. Global land cover classification at 1km spatial resolution using a classification tree approach. Int. J. Remote Sensing 21, 1331–1364.

Homer, C., Dewitz, J., Fry, J., Coan, M., Hossain, N., Larson, C., Herold, N., McKerrow, A., VanDriel, J., Wickham, J., 2007. Completion of the 2001 national land cover database for the counterminous United States. Photogrammetric Eng. Remote Sensing 73, 337–341.

Huete, A., Didan, K., Miura, T., Rodriguez, E.P., Gao, X., Ferreira, L.G., 2002. Overview of the radiometric and biophysical performance of the MODIS vegetation indices. Remote Sensing Environ. 83, 195–213.

Hüttich, C., Herold, M., Wegmann, M., Cord, A., Strohbach, B., Schmullius, C., Dech, S., 2011. Assessing effects of temporal compositing and varying observation periods for large-area land-cover mapping in semi-arid ecosystems: Implications for global monitoring. Remote Sensing Environ. 115, 2445–2459.

Jarvis, A., Reuter, H.I., Nels on, A., Guevara, E., 2008. Hole-filled SRTM for the globe Version 4, available from the CGIAR-CSI SRTM 90 m Database. (<http://srtm.csi.cgiar.org>).

Liang, L., Xu, B., Chen, Y.L., Liu, Y., Cao, W.C., Fang, L.Q., Feng, L.M., Goodchild, M.F., Gong, P., 2010. Combining spatial-temporal and phylogenetic analysis approaches for improved understanding on global H5N1 transmission. PLoS ONE 5 (10), e13575. http://dx.doi.org/10.1371/journal.pone.0013575.

Liu, D., Kelly, M., Gong, P., 2006. A spatial–temporal approach to monitoring forest disease spread using multi-temporal high spatial resolution imagery. Remote Sensing Environ. 101, 167–180.

Liu, D., Song, K., Townshend, J.R., Gong, P., 2008. Using local transition probability models in Markov random fields for forest change detection. Remote Sensing Environ. 112, 2222–2231.

Liu, D., Cai, S., 2012. A spatial-temporal modeling approach to reconstructing land-cover change trajectories from multi-temporal satellite imagery. Ann. Assoc. Am. Geogr. 102, 1329–1347.

Loveland, T.R., Reed, B.C., Brown, J.F., Ohlen, D.O., Zhu, Z., Yang, L., Merchant, J.W., 2000. Development of a global land cover characteristics database and IGBP DISCover from 1 km AVHRR data. Int. J. Remote Sensing 21, 1303–1330.

Schneider, A., Friedl, M.A., Potere, D., 2009. A new map of global urban extent from MODIS satellite data. Environ. Res. Lett. 4, 044003.

Schneider, A., Friedl, M.A., Potere, D., 2010. Mapping global urban areas using MODIS 500-m data: new methods and datasets based on 'urban ecoregions'. Remote Sensing Environ. 114, 1733–1746.

Si, Y., de Boer, W.F., Gong, P., 2013. Different environmental drivers of avian influenza outbreaks in poultry and wildbirds. PLoS One 8 (1), e53362. http://dx.doi.org/10.1371/journal.pone.0053362.

Sulla-Menashe, D., Friedl, M.A., Krankina, O.N., Baccini, A., Woodcock, C.E., Sibley, A., Sun, G.Q., Kharuk, V., Elsakov, V., 2011. Hierarchical mapping of Northern Eurasian land cover using MODIS data. Remote Sensing Environ. 115, 392–403.

Sun, F., Zhao, Y., Gong, P., Ma, R., Dai, Y., Remote sensing of dynamic land cover types: areal variation of major water bodies in China from 2001-2010 at a time scale of 8 days. Chinese Sci. Bull. (In preparation).

Tateishi, R., Uriyangqai, B., Al-Bilbisi, H., Ma, Ghar, Tsend-Ayush, J., Kobayashi, T., Kasimu, A., Hoan, Nt., Shalaby, A., Alsaaideh, B., Enkhzaya, T., Gegentana, Sato, H.P., 2011. Production of global land cover, GLCNMO. Int. J. Digital Earth 4, 22–49.

Thenkabail, P.S., Biradar, C.M., Noojipady, P., Dheeravath, V., Li, Y.J., Velpuri, M., Gumma, M., Reddy, G.P.O., Turral, H., Cai, X.L., Vithanage, J., Schull, M., Dutta, R., 2009. Global irrigated area map (GIAM), derived from remote sensing, for the end of the last millenium. Int. J. Remote Sensing 30, 3679–3733.

Townshend, J.R.G., Masek, J.G., Huang, C.Q., Vermote, E.F., Gao, F., Channan, S., Jo, Sexton, Feng, M., Narasimhan, R., Kim, D., Song, K., Song, D.X., Song, X.P., Noojipady, P., Tan, B., Hansen, M.C., Li, M.X., Wolfe, R.E., 2012. Global characterization and monitoring of forest cover using Landsat data: opportunities and challenges. Int. J. Digital Earth 5, 373–397.

Waring, R.H., Coops, N.C., Fan, W., Nightingale, J.M., 2006. MODIS enhanced vegetation index predicts tree species richness across forested ecoregions in the contiguous USA. Remote Sensing Environ. 103, 218–226.

Wu, T.F., Lin, C.J., Weng, R.C., 2004. Probability estimates for multi-class classification by pairwise coupling. J. Mach. Learn. Res. 5, 975–1005.

Xiao, X., Shen, Z., Qin, X., 2001. Assessing the potential of VEGETATION sensor data for mapping snow and ice cover: a normalized difference snow and ice index. Int. J. Remote Sensing 22, 2479–2487.

Yang, J., Gong, P., Fu, R., et al., 2013. The role of satellite remote sensing in climate change studies. Nat. Climate Change 3, 875–883.

You, L., Wood, S., Wood-Sichra, U., 2009. Generating plausible crop distribution maps for Sub-Saharan Africa using a spatially disaggregated data fusion and optimization approach. Agric. Syst. 99, 126–140.

Yu, L., Wang, J., Gong, P., 2013a. Improving 30 m global land-cover map FROM-GLC with time series MODIS and auxiliary data sets: a segmentation-based approach. Int. J. Remote Sensing 34, 5851–5867.

Yu, L., Wang, J., Clinton, N., Xin, Q., Zhong, L., Chen, Y., Gong, P., 2013b. FROM-GC: 30 m global cropland extent derived through multi-source data integration. Int. J. Digital Earth 6, 521–533.

Zhao Y., Gong P., Yu L., et al. A common validation sample set for global land cover mapping. Int. J. Remote Sensing (submitted for publication).